Uniformity Control in Sputter Deposition Processes

W. De Bosscher, Bekaert Advanced Coatings, Deinze, Belgium; A. Blondeel, Bekaert VDS, Deinze, Belgium; and G. Buyle, State University of Ghent, Ghent, Belgium

Key Words: Sputter deposition, Cylindrical targets, Magnetron design, PVD sources

ABSTRACT

Magnetron sputtering, combined with an accurate control of process parameters and layer quality, has proven to be one of the most important methods for thin film deposition. The major shortcomings of this technique (e.g. low target utilization and limited sputter yield) could be largely overcome by the introduction of cylindrical magnetrons with rotating target tubes. However, the recent introduction of complex coating stacks on rigid (e.g. glass) and flexible (e.g. polymer substrates) large area substrates for advanced automotive, architectural and display applications demands stringent requirements of the deposition process. One of the primary challenges is the uniform controlled deposition of both thin metal and metal oxide/nitride films on large area or high volume products.

In this paper, the impact of several sputter components on coating uniformity is reviewed. The magnet system of a stand-alone magnetron is the predominant factor for uniformity over the substrate width. Experimental and simulation results of changing the magnetic configuration on magnetic field strength and film thickness are presented. A new approach for the angular distribution of ejected sputter particles is presented. A simple formula, in which a real physical meaning is given to each term, allows fast and accurate prediction of angle and target voltage dependent sputter yield. Additional uniformity effects by closely spaced magnetrons and the influence of anodes are discussed as well. A simple and effective technique for improving the layer thickness uniformity by adjusting the magnetic field strength locally is presented.

INTRODUCTION

Over the last few decades, magnetron sputtering has become one of the most important methods for depositing thin films. Some of the key features for supporting this success are:

- relative ease of scaling to larger dimensions
- high mass productivity (high deposition rate)
- good control of thickness and quality uniformity
- wide variety of available materials to be sputtered

In addition, the number and magnitude of applications incorporating thin film technologies is growing rapidly [1]. The main fields and most important applications for magnetron sputter deposition are:

- microelectronics: conductors, adhesion/barrier/AR
- advanced display: AR for CRT, TCO for flat panels
- architectural: low-E and solar control glass
- automotive: low-E, privacy glass, electrochromics
- data storage: magnetic, optical and combined
- optical: AR lenses, filters, mirrors

In all of these fields, a well-designed stack of multiple thin layers consisting of pure metals, alloys, oxides or nitrides, only achieves the desired functionality of the coating. Good control of each separate deposition process, including layer thickness, quality and dedicated specifications (optical, electrical, mechanical, …) is essential. Large area deposition processing pushes extreme controllability even further requiring all of these optimal properties in a short and long term reproducible way and uniformly over the substrate width.

Sputter deposition of metals and metallic alloys is quite straightforward and is mainly defined by the quality of the target material and the magnetron configuration. The deposition process of nitrides and the even more insulating oxides has evolved significantly over the past few decades. Although RF-powered magnetrons allow the sputtering from compound ceramic targets, this technique remains difficult to scale-up. As a result, pure DC and, if necessary, pulsed DC or AC-switching with frequencies below 100 kHz seem the successful ways to proceed for reactive sputtering. To achieve relative high deposition rates, the target should remain in metallic mode while the oxide or nitride compound layer is being formed on the substrate by controlled addition of oxygen or nitrogen in the vacuum chamber during the sputter process. Moreover, sub- and superstoichiometric layer composition may be obtained by appropriate tuning of gas flow and sputter parameters.

During the deposition process, the insulating compound layer is simultaneously formed on the substrate, the chamber walls, the anodes and on the target surface besides the erosion zone. Especially the latter may cause severe arcing problems, resulting in process destabilization and potential physical damage

45th Annual Technical Conference Proceedings (2002) ISSN 0737-5921

to target, anodes and substrate. At present, power supplies are equipped with arc detection and interrupt circuitry to limit the amount of energy dissipated into the arc. The last decade offered new solutions for this problem [2]. Besides standard planar targets, the cylindrical rotating magnetron was successfully introduced on industrial scale.

This concept, as depicted in Figure 1, offers far superior properties and accommodates most of industrial requirements. In comparison to planar targets it offers:

- very high target utilization (up to 90%)
- more material on limited target dimensions
- higher power densities because of effective cooling
- higher stability in reactive sputter processing
- more efficient in AC switching (anode function)

As a result, higher throughput, more complex layer stacks and larger uninterrupted stable production cycles with constant quality may be achieved.

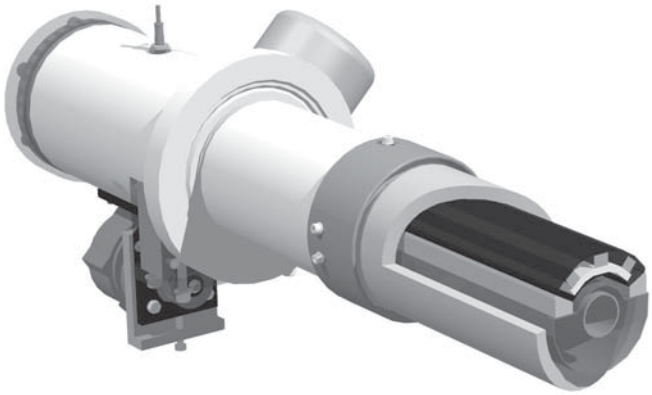

Figure 1: Cylindrical magnetron with cutout target tube and new adjustable Flextrak® magnet bar configuration

EXPERIMENTAL

Over the past few years, a theoretical fuzzy-logic computer model for magnetron sputtering has been developed. The model contains several linked modules of which a few new ones are used for this project. Earlier we developed two modules; one for the calculation of the spatial magnetic field distribution for a given magnet configuration and another for the calculation of the plasma density and energy above a powered target within a magnetic field. A combination of both existing modules allows one to predict the groove formation in the target as a result of a given magnet set-up. The simulation software is based on pure analytical integrating models and not on finite element analysis nor on Monte-Carlo simulations. As a result, calculation time may be reduced without losing accuracy. The fuzzy-logic part of the simulation keeps track with the target topology and field strength at every instance of the erosion process. An excellent correlation between simulation and target erosion profile was obtained earlier during the successful development of the Cyclomag®. In this case, the magnet array is moved below a planar target in such a way that an over-all utilization of more than 60% may be realized [3]. A new software module calculates an appropriate spatial material density distribution of sputtered particles at the target surface. The module takes into account the properties of the sputtering gas (mass, angle of incidence and energy) and properties of the target material (mass, density, surface and bulk binding energies). This module is based on the work of Biersack [4] and uses a finite element calculation method. As a result, the Monte Carlo simulation easily takes 100 times longer on the same computer than each other module separately. A combination of the prior modules and the new angular density module allows the complete modelling of all particles leaving the target surface. Within yet another new module, the partial pressures of the most important species in the vacuum chamber between target and substrate are taken into account for calculating the mean free path length and the effect of an interaction. The final result is a material thickness and uniformity distribution over the substrate surface. In addition, a mapping of the energy of the arriving particles on the substrate may be generated as well.

Experimental verification of the complete thickness distribution model was performed in a test chamber and using a newly in-house developed 200 mm circular magnetron. This magnetron is depicted in Figure 2 and allows the free positioning of all magnets below the target.

Figure 2: Planar magnetron for 8" circular targets and with complete freedom for positioning magnets

Sputter experiments with magnet configurations generating both circular and square racetracks and with diameters ranging from 50 to 150 mm were performed. Target-substrate spacing was typically set between 50 and 100 mm in a pressure range from 0.1 to 0.5 Pa. In a stationary condition (no movement between substrate and magnetron) layers were deposited in a metallic deposition mode and with a thickness close to 1 μm. Microscope quartz plates were prepared before deposition to allow easy step measurement with a Dektak IIA after the sputter process. A mapping of these thickness measurements was compared with the simulation results.

In the meantime, a new concept magnet array for rotating cylindrical magnetrons was designed and constructed. An important feature of the Flextrak® configuration is the ability of positioning magnets at any desired location on a cylindrical segment. This can be seen in Figure 1 (right-hand side) and was discussed earlier in more detail [5]. Over the magnet configuration a sealing thin-walled tube segment is placed. Eliminating the interaction between the magnetic material and the cooling water gives much better magnetic integrity and sustains the purity of the cooling water. Moreover, the cooling water is conducted between the protection tube and the inner target tube envelope, giving an optimal heat transfer and cooling efficiency. At present, the Flextrak® magnet bar is further improved and brought to a new level of performance. While maintaining all previous properties, the magnetic field strength may be tuned locally with sub-percentage precision. This can be performed in a fast, user-friendly and reproducible way and does not need to break the water/magnet seals. Two of those adjustable Flextrak® magnet bars were installed inside 152" Sn target tubes and tested in a dual rotatable magnetron configuration. Both metallic and reactive sputter experiments with DC and AC power supplies were performed. These tests were executed in our full-sized test chamber (see Figure 3). Small glass substrates were moved back and forth over a sputter window of 300 mm at a speed of 1 m/min. The number of passes was 10 for metallic and 20 for reactive processes to obtain a sufficiently thick layer for Dektak measurements.

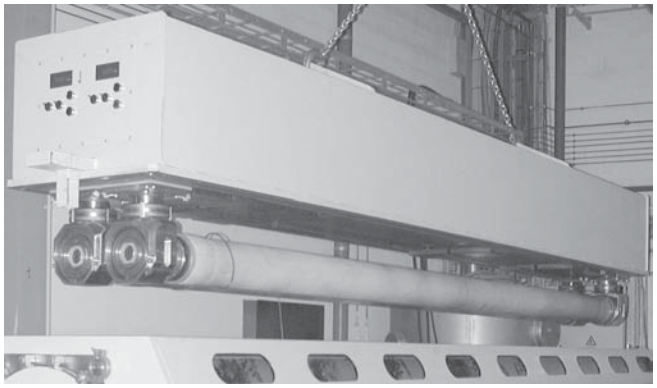

Figure 3: Experimental set-up for large area uniformity testing containing a dual rotatable magnetron

RESULTS

In the course of this research project both theoretical (simulation) and experimental work was performed. Both results were always in good agreement for single magnetron configurations under metallic sputter deposition conditions. Slight differences were used to refine or better understand the simulation model. More complex experimental results were obtained in closely spaced dual rotatable magnetron configurations. Further perturbations in layer quality and thickness uniformity were observed in reactive deposition processes with additional effects of mid frequency AC mode.

Earlier work has proven that our simulation model for calculating the exact erosion groove profile for a given target surface topography and magnet array position is quite successful [3]. This information was used as a weighting factor for the number of incident Ar^+-ions as a function of the position on the target. Consequently, the finite element module was used for calculating the angular distribution of ejected target particles. The simulation contains one million of normal incident Ar^+-ions on a Ti-target (left) and Si-target (right) to obtain a high level of accuracy and is depicted in Figure 4.

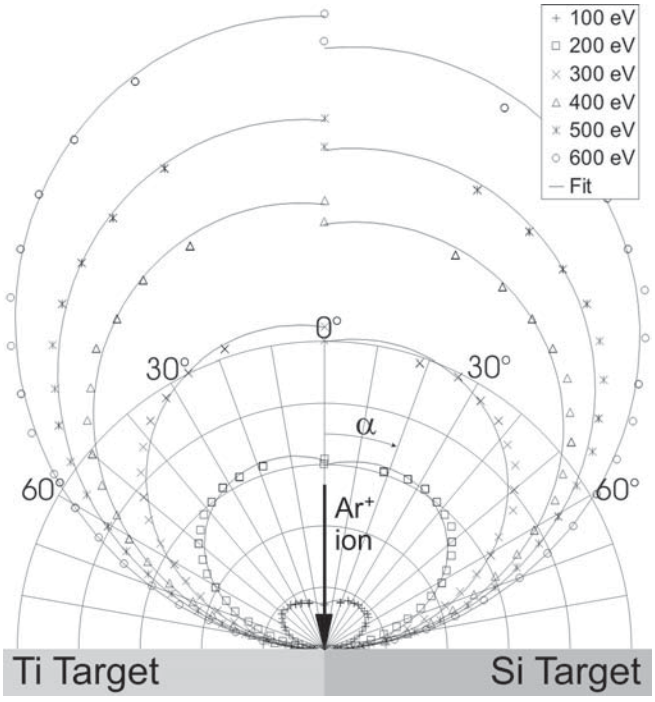

Figure 4: Angular distribution (in spherical coordinates) for ejected Ti (left) and Si (right) target particles and for perpendicular incident Ar^+-ions with energies ranging from 100 eV to 600 eV

This module remains however quite impractical because of the need of very long calculation times in comparison to all other modules, which are based on pure analytical and physical models. To overcome this problem, a simple 2 parameter fit formula was generated and is depicted in Figure 4 as well for both Ti and Si. The fit formula corresponds nicely with the finite element simulation for all angles and energies. By this operation, several hours of calculation time is reduced to a fraction of a second. Furthermore, in contrast to the Monte Carlo simulation, which has to be performed for any discrete set of conditions, the fit formula can generate instantaneously a sputter yield for any given angle and target voltage.

These results were further combined with the particle-in-flight module, taking into account the possible interactions during the trajectory from target to destination.

The comparison between the final result of the simulation package and the lab-scale experiments with the 8" circular magnetron containing various magnet configurations was striking. In a very specific request, we had to coat a 4" on 4" square substrate with the 8" circular magnetron. The desired uniformity over the complete substrate was ± 1.5%. We were able to calculate the optimal magnetic configuration for a given target thickness, target-substrate spacing and gas pressure. The real experimental test results with the calculated settings were virtually identical, even the thickness gradient of the coating on the side shields corresponded well with the simulation. After entering all the variables in each of the four linked modules, the complete calculation time of the erosion profile on the target and the thickness uniformity profile on the substrate takes typically 10 minutes.

Transfer of the simulation package from planar to rotating cylindrical magnetrons requires minor adjustments. Since the rotating target tube does not exhibit any racetrack and since it is assumed that all ions reach the target normal to its surface, the particle ejection module is simplified to cylindrical target topography. Furthermore, typically for the large area coating environment, the moving substrate is introduced. This is easily mathematically incorporated by a line integration of the stationary thickness profile along the direction of the substrate movement. Similar simulations were performed earlier [5] for moving substrates in front of planar and rotating cylindrical magnetrons and for various racetrack turns. The different magnetron conditions and the according relative coating thickness simulations as a function of the substrate position relative to the magnetron edge are shown in Figure 5. The large extent of the thickness gradient is the result of a light target atom, large substrate-target spacing and the relative high gas pressure. It is quite logical that the resulting layer thickness on the substrate at the edge of the magnetron is substantially reduced because of the finiteness of the target tube. Similar results were found in large area coating experiments for single magnetron configurations and for symmetric set-up for shielding and/or anodes at both sides along the target length.

However, the story becomes totally different from the moment that the symmetry is not maintained. It is known [6] that an anode along a single side of a rotating cylindrical magnetron severely disturbs the coating uniformity. A typical sputter configuration in which 2 similar magnetrons are spaced sufficiently close to each other (e.g. see Figure 3), has an important influence on the coating uniformity as well. Reactive sputtering and/or AC switching between the target tubes may introduce even further distortions of the coating uniformity. The dotted line in Figure 6 (Neutral) represents the coating uniformity over 3200 mm for a reactive AC sputter process of 152" Sn-tubes in an Ar/O_2 gas mixture. Tuning of the magnetic field strength in the adjustable Flextrak® magnet bar allows one to compensate the ± 20% non-uniformity and realize a ± 1.5% uniformity.

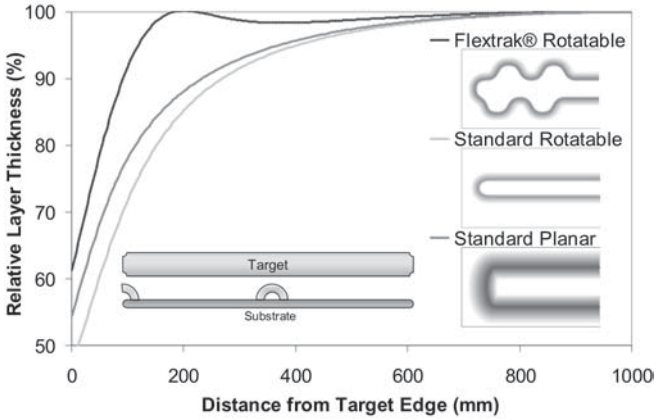

Figure 5: Relative layer thickness simulation on a substrate 100 mm above Al target for sputtering in Ar at 0.4 Pa by using different racetrack configurations

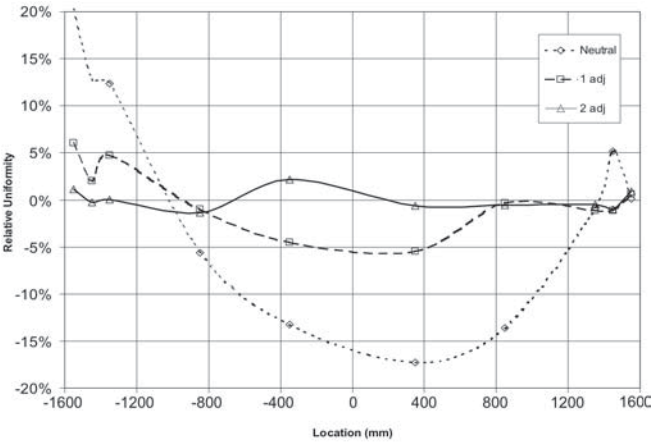

Figure 6: Layer thickness uniformity of SnO_2 layers over a substrate width of 3200 mm for a neutral and 2 subsequent regulation settings of the adjustable Flextrak® magnet bar

DISCUSSION

The first set of experiments, performed in the lab-scale coater with the 8" circular magnetron, was mainly focussed on understanding all the main parameters influencing layer thickness uniformity. The availability of the extremely flexible in-house developed magnetron was very helpful. The impact of various balanced and unbalanced magnet configurations on erosion profile and target utilization could be monitored. This has proven to be an indispensable tool for verifying the corresponding simulation modules. The main effects playing a role in target erosion for metallic process single magnetron symmetric configurations are now well understood. As a result, the simulation model could be refined and allows now quite accurate prediction of racetrack and erosion groove. However, the main goal of the complete simulation package is a full prediction of layer thickness and quality distribution on a substrate for a given geometry and gas condition. Here again, the lab-scale coater and thickness measurements are used for verifying the simulation results. The results on the 4'*4" square substrates proved that not only the sputter process on the target, but also the deposition process on the substrate could be simulated quite accurately. Showstopper in the calculation software was clearly the finite element module for angular distribution of ejected particles, which was extremely slow and could not be integrated automatically with the other modules. Generating beforehand value tables of ejected intensities for a given material, ion energy and angle is possible but remains difficult to handle because it is a massive work and interpolation is not straightforward. Over the last 4 decades a lot of scientific work has been published to solve the distribution into a simple equation. Quite known is the approach of an under-cosine distribution for low energies (< 0.1 keV) transforming to an over-cosine for high energies (> 1 keV) [7]. Absolute intensities were not defined, only the shape is given. More recent work [8] tries to fit the distribution with a $\cos^n(\alpha)$ function, but focuses on Ar^+-ion energies between 1 en 10 keV and the exponent n is defined by some physical parameters and 3 fitting parameters. A valuable solution for typical magnetron sputter conditions was not found. Because of that, we tried to generate a simple fit formula with a minimum of variables, an optimal fit to the Monte Carlo results and, as a cherry on the cake, with a real physical meaning of each term in the formula. A consistent fitting formula for each material may be generated and Figure 4 shows the result for Ti and Si targets. For this discussion, we will limit ourselves to the fit formula for Si; however, the same principle is valid for all materials. The angular and Ar^+-ion energy dependent yield Y of ejected Si particles is given by:

$$Y = a*\cos^{1.3}(\alpha) + b*\sin\{\alpha*[0.69*(\alpha - \pi/2) + 2]\}$$

In this formula we can distinguish a cosine term with a fixed exponent higher than one, giving an over-cosine distribution. The sine term appears slightly more complex, but is based on a $\sin(2\alpha)$ distribution. This function generates a lobe in spherical coordinates with a maximum at 45° and being 0 at 0° and 90°. The portion in the sine function with the 0.69 factor is only intended to shift the lobe in such a way that the maximum occurs at 54°. Equal portions of the cosine and sine term will generate a heart-shaped distribution as can be found for the 100 eV points in Figure 4. The formula contains only 2 fitting parameters, representing the coefficients of each term. The fitting parameters a and b are angle α independent and vary only with the incident Ar^+-ion energy E as shown in Figure 7.

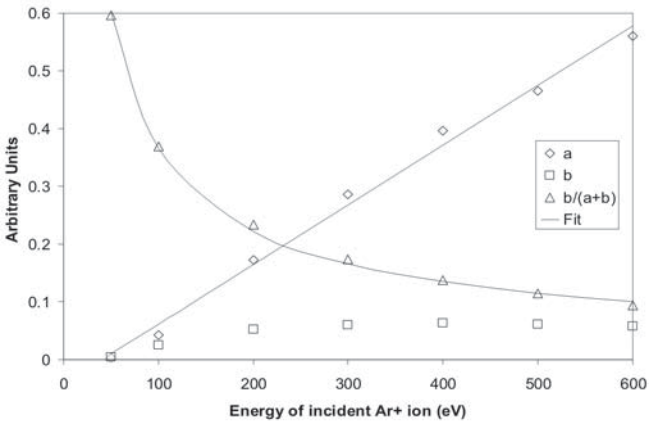

Figure 7: Variation of fitting parameters a, b and b/(a+b) as a function of incident Ar^+-ion energy

Out of the fitting lines we can conclude that the cosine term is quite linearly proportional with the ion energy E, while the contribution of the sine term in the formula (i.e. b/(a+b)) decreases proportionally with $E^{-0.9}$ for increasing ion energy. The sine term may be attributed to Ar-Si interactions at the surface of the target and is defined by the surface binding energy. As a result, at very low Ar energies (< 50 eV), only the surface layers of the target material feel the interaction and due to the limited collision cascade a $\sin(2\alpha)$-like distribution is observed. At higher Ar energies, an interaction takes place with the target bulk material and the collision cascade becomes much more complex. In this case, target atoms that leave the surface are generated primarily below the surface and generate a typical cosine distribution. The surface interaction saturates for an Ar^+-ion energy of a few hundred eV (see b coefficient in Figure 7) while the number of particles generated in the bulk of the target material increases proportional with the Ar^+-ion energy (see a coefficient in Figure 7). The exponent on the cosine term is dependent on target material and incident species but is always larger than 1. The angle of maximum intensity in the sine term varies with target material and incident species as well. However for each target/ion combination, these values are fixed and a simple energy dependent correlation may be found for the fit parameters a and b/(a+b). This method proved to be successful for all tested materials and for Ar^+-ion energies ranging from 50 to 600 eV.

In a second set of experiments, we tried to transfer the successful results from the lab coater experiments to large-scale rotatable magnetrons with moving substrates. Although the powerful simulation software could be adapted quite easily to this set-up, only good correlation results were obtained for single magnetrons and with a symmetric configuration of shields and anodes. This situation is often valid in web coaters and was tested with our cantilevered magnetrons (see Figure 1). Confirmation of the simulation results from Figure 5 was found in the coating uniformity profiles on polyester and steel webs. From the moment a single anode was placed on one side of the target tube, the uniform thickness profile from before changed drastically into an enormous gradient from left to right over the substrate width. Moving the single anode to the other side of the target tube inverts this gradient. The origin of this distortion can be found in electrons leaving the plasma in one of the turns at the target tube end to be collected by the single sided anode [6]. The electrons are lost at the opposite racetrack turn when the anode is moved to the other side of the target. A similar effect occurs when two closely spaced magnetrons are operated either in DC or in AC mode. Although the effect on target erosion and layer thickness uniformity is different for each mode, a non-uniform erosion and layer thickness gradient may be observed for each target tube separately. In fact, every powered cathode sees a different space charge region at each side; one side contains another target at negative potential (in DC mode) or positive potential (AC mode), while the other side consists of grounded shields and chamber walls or in DC mode possibly an anode. The magnetic field strength uniformity of the Flextrak® magnet configuration was within ± 2% over the complete length of the target tube for the "Neutral" dotted curve in Figure 6. Although this magnet configuration gave uniform coating results in single symmetric magnetron set-ups, a non-uniformity of ± 20% is obtained in the reactive AC set-up for depositing SnO_2 layers. Two uniformity-perturbing effects may be distinguished. Firstly, in contrast to the single magnetron configuration, the thickness at the edges of the substrate is higher than in the middle. Secondly, the profile is not symmetric with respect to the centre (0 location in Figure 6) of the substrate. The reactive gas flow was kept uniform over the target length during all deposition experiments. Similar results were also obtained for pure metallic tests in AC mode, proving that the gas and pumping configuration is not the dominant origin of the non-uniformity. Furthermore, it is clear that the large layer thickness non-uniformity is not primarily caused by the magnetic field configuration on itself, but by plasma interactions on and in the close neighborhood of the magnetron. The new adjustable Flextrak® magnet bar gives the possibility to adjust the magnetic field strength locally without breaking the water seal integrity of the magnet configuration. The tuning accuracy is very high and each local setting may be quantified to allow easy reproducibility on other adjustable magnet bars as well. Each side of the linear racetrack along the target tube length may be regulated separately. Although a very uniform magnetic field strength over the target length may be achieved with this system, the real strength of the concept lays in the ability to (de)tune the field in such a way that local thickness non-uniformities get compensated. An initial correction of the neutral magnetic field strength improves the layer thickness uniformity from ± 20% to ± 5%, as can be seen by the dashed line in Figure 6. The second adjustment of the Flextrak® magnet bar, represented by the solid line in Figure 6, is already slightly overcompensated but shows that a tuning for achieving a ± 1.5% layer thickness and quality uniformity is feasible. This example shows that a peak-to-peak layer thickness gradient of about 40% may be corrected by the adjustable Flextrak® magnet bar. It should be clear that the magnetic regulation does not really suppress the plasma instabilities, but generates a non-uniform sputter yield over the target length that exactly compensates the uniformity deviations. The magnitude of plasma instabilities and the degree of required magnetic compensation with the adjustable magnet bar depend mainly on the electrical field distribution, gas distribution and mechanical geometry in the sputter chamber.

CONCLUSIONS

All the different crucial aspects of the magnetron sputter deposition process have been studied. The results of earlier work with respect to magnetic and electric configurations and the effect on racetrack and erosion groove formation, were integrated in this project. Major attention in this paper has been paid to the angular distribution of ejected sputter particles. Monte-Carlo simulation results were simplified to an analytical formula. A physical meaning could be given to every component in the formula and the relative importance of each term as a function of target voltage was highlighted and explained. This information was integrated in a complete sputter simulation package that allows one to calculate the layer thickness uniformity. Parallel to this, the validity of each simulation module was verified by relevant sputter tests in a well-controlled lab-scale coater. The good agreement between simulation results and thickness uniformity measurements from lab-scale and industrial large-area experiments proves that a good understanding of the metallic symmetric DC sputter process is acquired.

Additional experiments in a dual magnetron set-up, using AC switching power supplies and for a reactive deposition process shows that the previous understanding is insufficient for explaining the observed uniformity behavior. Plasma gradients, due to AC-mode and instabilities due to non-symmetric spatial distributions need further research for a better understanding. However, the large non-uniformities that we obtained in these processes may be corrected by introducing the new adjustable Flextrak® magnet bar. This system offers the possibility to adjust the magnetic field strength locally in an easy and user-friendly tuning mechanism. The regulation window is quite large while the accuracy remains high.

REFERENCES

1. M. Rittner, Sol. St. Technol., 43, nr. 1, 24 (2000).

2. K. Suzuki, Proc. 2nd ICCG, 24 (1998).

3. W. De Bosscher, H. Lievens, Thin Solid Films, 351, 15 (1999).

4. J.P. Biersack, W. Eckstein, Appl. Phys. A, 34, 73 (1984).

5. W. De Bosscher, D. Cnockaert, H. Lievens, SVC 42nd ATCP, 156 (1999).

6. P. Sieck, U.S. Pat. # 5,645,699 (Jul. 08, 1997).

7. E. Kay, Adv. Electronics and Electron Phys., 17, 245 (1962).

8. V.I. Shulga, Nucl. Instr. And Meth. B, 164, 733 (2000).